Nanoelectromechanical Systems: Experiments and Modeling

1. Introduction

Nanoelectromechanical systems (NEMSs) are systems with characteristic dimensions of a few nanometers. By exploiting nanoscale effects, NEMSs present interesting and unique characteristics, which deviate greatly from their predecessor microelectromechanical systems (MEMSs). For instance, NEMS-based devices can have fundamental frequencies in the microwave range ($\sim$100 GH) (Rueckes *et al*. 2000); mechanical quality factors in the tens of thousands (ultralow energy dissipation); active mass in the femtogram range; force sensitivity at the attonewton level; mass sensitivity up to attogram (Ilic *et al*. 2000) and subattogram (Davis *et al*. 2000) levels; heat capacities far below a "yoctocalorie" (Roukes 1999); power consumption in the order of 10 aw (Roukes 2004); and extreme high integration level, approaching 10^{12} elements per cm^2 (Rueckes *et al*. 2000). All these distinguishing properties of NEMS devices pave the way to applications such as force sensors, chemical sensors, biological sensors, and ultrahigh frequency resonators.

The interesting properties of the NEMS devices typically arise from the behavior of the active parts, which, in most cases, are in the forms of cantilevers or doubly clamped beams with dimensions at the nanometer scale. The materials for those active components include silicon, silicon carbide, carbon nanotubes, gold and platinum, to name a few. Silicon, the basic material employed in integrated circuit (IC) technology and MEMS, has been widely used to build NEMS. However, ultrasmall silicon-based NEMS nanoresonators failed to achieve the much anticipated high-quality factors due to the dominance of surface effects, such as surface oxidation and reconstruction, and thermoelastic damping. Limitations in strength and flexibility also compromise the performance of silicon-based NEMS actuators. Instead, carbon nanotubes appear to be ideal for NEMS given their nearly one-dimensional structures with high aspect ratio and nearly perfect-terminated surfaces and excellent electrical and mechanical properties. Due to significant advances in growth, manipulation, knowledge of electrical and mechanical properties, carbon nanotubes have become the most promising building blocks for the next generation of NEMS. Several carbon-nanotube-based functional NEMS devices have been reported so far (Kim and Lieber 1999, Rueckes *et al*. 2000, Akita *et al*. 2001, Fennimore *et al*. 2003, Kinaret *et al*. 2003, Ke and Espinosa 2004, Sazonova *et al*. 2004). Similarly to carbon nanotubes, nanowires are a type of one-dimensional novel nanostructure well suited for building NEMS because of their size and controllable electrical properties.

The purpose of this article is to provide a review of NEMS devices to date and to summarize the modeling currently being pursued to gain insight into their performance. This article is organized as follows: in the first part, we review carbon-nanotube- and -nanowire-based NEMS. In the second part, we present the multiphysics modeling of NEMS based on continuum theory.

2. NEMS

2.1 Carbon-nanotube-based NEMS Devices

(a) Nonvolatile random access memory (NRAM). A carbon-nanotube-based nonvolatile random access memory (NRAM) reported by Rueckes *et al*. (2000) is illustrated in Fig. 1. The device is a suspended SWNT crossbar array for both I/O and switchable, bistable device elements with well-defined OFF and ON states. Qualitatively, bistability can be envisioned as arising from the interplay of the elastic energy and the van der Waals energy when the upper
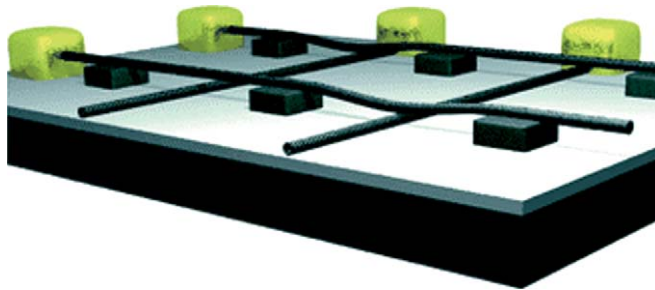

Figure 1
Schematics of free-standing nanotube device architecture with multiplex addressing. Reprinted with permission from Rueckes T, *et al*. 2000 Carbon nanotube-based nonvolatile random access memory for molecular computing. *Science* **289**, 94–7. Copyright 2000 AAAS.

nanotube is freestanding or the suspended SWNT is deflected and in contact with the lower nanotube. For a device element, these two states can be read easily by measuring the resistance of the junction. Moreover, it can be switched between OFF and ON states by applying voltage pulses to produce attractive or repulsive electrostatic forces. A key aspect of this device is that the separation between top and bottom conductors must be of the order of 10 nm. In such case, the van der Waals energy overcomes the elastic energy when the junction is actuated (ON state) and remains on this state even if the electrical field is turned off (nonvolatile feature). With multiplexing, this device is envisioned to function as a highly integrated ($\sim 1 \times 10^{12}$ elements per square centimeter), fast (~ 200 GHz operation frequency), and macroscopically addressable nonvolatile random access memory (RAM) structure that could overcome the fundamental limitations of semiconductor RAM in size, speed, and cost. However, small junction gap sizes impose significant challenges in the nanofabrication of parallel device arrays.

(b) Nanotweezers. There are two types of carbon-nanotube-based nanotweezers reported by Kim and Lieber (1999) and Akita *et al.* (2001), respectively.

Both nanotweezers employ multiwalled carbon nanotubes (MWNTs) as tweezers' arms which are actuated by electrostatic forces. The applications of these nanotweezers include the manipulation of nanostructures and two-tip STM or AFM probes (Kim and Lieber 1999). Figures 2(a)–2(d) show the motion of the nanotube arms as a function of the applied voltage V (Akita *et al.* 2001). In this sequence of images, it is clearly seen that the arms bent and the separation between the tips decreased with increasing applied voltage. The separation became 500 nm at $V = 4$ V and zero at $V > 4.5$ V. The authors noted that the motion shown in Figs. 2(a)–(d) could be repeated many times without any permanent deformation, showing that carbon nanotubes are ideal materials for building NEMSs.

(c) Rotational motors. A carbon-nanotube-based rotational motor reported by Fennimore *et al.* (2003) is conceptually illustrated in Fig. 3. The rotational element (R), a solid rectangular metal plate serving as a rotor, is attached transversely to a suspended support shaft which ends are embedded in electrically conducting anchors (A1, A2) that rest on the oxidized surface of a silicon chip. The rotor plate assembly is surrounded by three fixed stator electrodes (S1, S2,
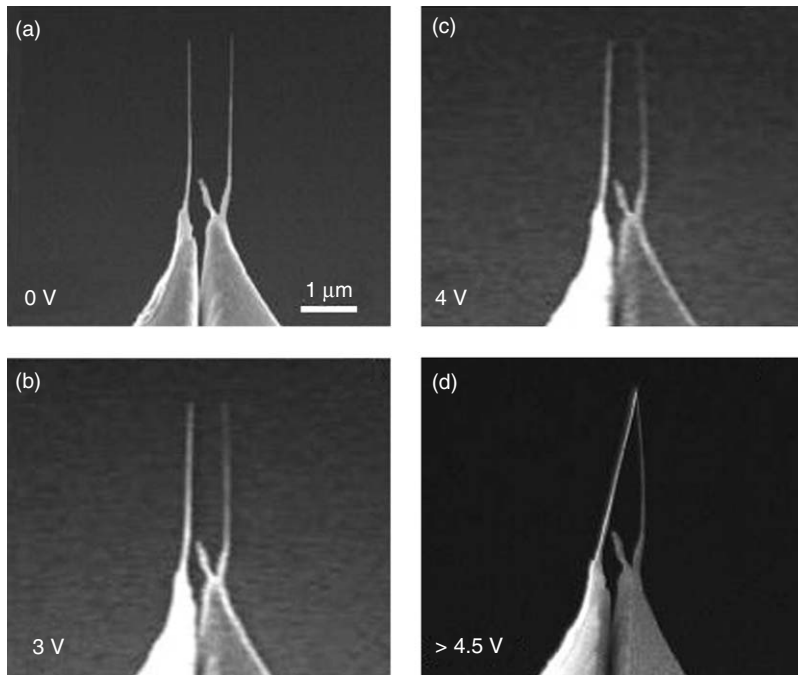

Figure 2
SEM images of the motion of nanotube arms in a pair of nanotweezers as a function of the applied voltage. Reprinted with permission from Akita S, *et al.* 2001 Nanotweezers consisting of carbon nanotubes operating in an atomic force microscope. *Appl. Phys. Lett.* **79**, 1691–3. Copyright 2001, American Institute of Physics.

S3). Four independent (DC and/or appropriately phased AC) voltage signals, one to the rotor plate and three to the stators, are applied to control the position, speed, and direction of rotation of the rotor plate. The key component in the assembly is a single MWNT, which serves simultaneously as the rotor plate support shaft and the electrical feed-through to the rotor plate; most importantly, it is also the source of rotational freedom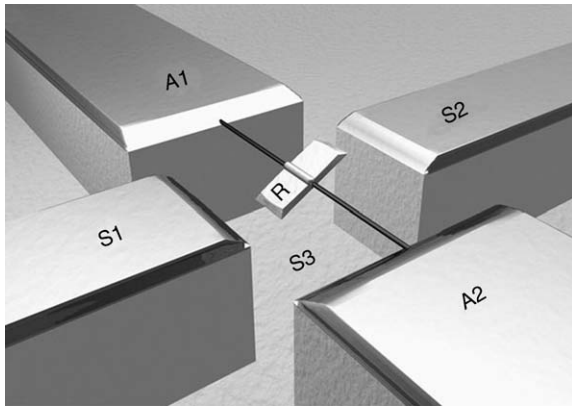. The experiments show that the MWNT clearly serves as a reliable, presumably wear-free, NEMS element providing rotational freedom. No apparent wear or degradation in performance was observed after many thousands of cycles of rotations. The potential applications of the actuators include ultrahigh-density optical sweeping and switching elements.

(d) Tunable oscillators. A tunable carbon nanotube oscillator was reported by Sazonova *et al.* (2004). It consists of a doubly clamped nanotube, as shown in Fig. 4. Single- or few-walled nanotubes with diameters in the range of 1–4 nm, grown by chemical vapor deposition (CVD) were suspended over a trench between two metal electrodes. The nanotube motion was induced and detected using the electrostatic interaction with the gate electrode underneath the tube. In this device, the gate voltage has both a static (DC) component and a small time-varying (AC) component. The DC voltage at the gate produces a static force on the nanotube that can be used to control its tension, therefore the oscillation frequency. The AC voltage produces a periodic electric force, which sets the nanotube into motion. As the driving frequency approaches the resonance frequency of the tube, the displacement becomes large. The device showed a high force sensitivity (below 5 aN), which made it a small force transducer.

(e) Nanorelays. Carbon-nanotube-based nanorelays were firstly reported by Kinaret *et al.* (2003) and later experimentally demonstrated by Lee *et al.*
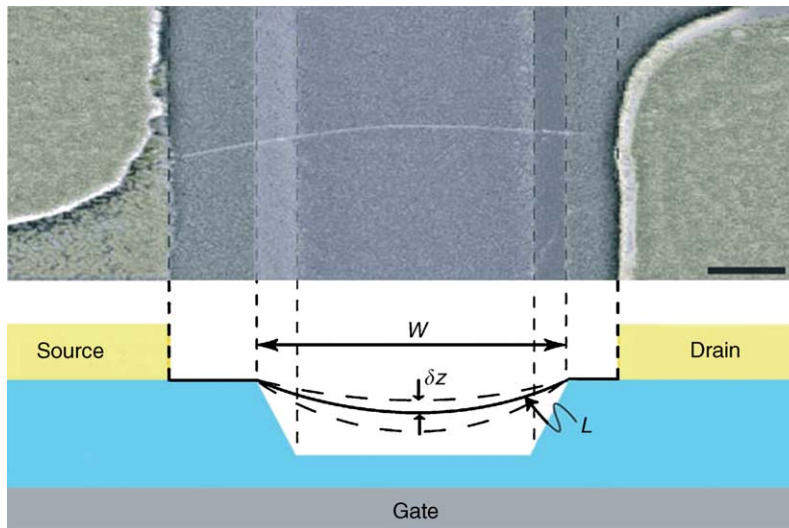

Figure 3
Conceptual drawing of the integrated synthetic NEMS actuator. Reproduced from Fennimore A M, *et al.* 2003 Rotational actuators based on carbon nanotubes. *Nature* **424**, 408–10, with permission from Nature Publishing Group.

Figure 4
SEM image of a suspended device (top) and a schematic of device geometry (bottom). Scale bar, 300 nm. Reproduced from Sazonova V, *et al.* 2004 A tunable carbon nanotube electromechanical oscillator. *Nature* **431**, 284–7, with permission from Nature Publishing Group.

(2004). The nanorelay is a three-terminal device including a conducting carbon nanotube placed on a terrace in a silicon substrate and connected to a fixed source electrode (S), as shown in Fig. 5. A gate electrode (G) is positioned underneath the nanotube so that charge can be induced in the nanotube by applying a gate voltage. The resulting electrostatic force brings the tube end into contact with a drain electrode (D) on the lower terrace, thereby closing an electric circuit. Theoretical modeling of the device shows that there is a sharp transition from a non-conducting (OFF) to a conducting (ON) state when the gate voltage is varied at a fixed source-drain voltage. The sharp switching curve allows for amplification of weak signals superimposed on the gate voltage (Kinaret *et al.* 2003).

(f) Feedback-controlled nanocantilevers. A feedback-controlled carbon-nanotube-based NEMS device reported by Ke and Espinosa (2004), schematically shown in Fig. 6, is made of an MWNT placed as a cantilever over a microfabricated step. The device has two well-defined stable equilibrium positions
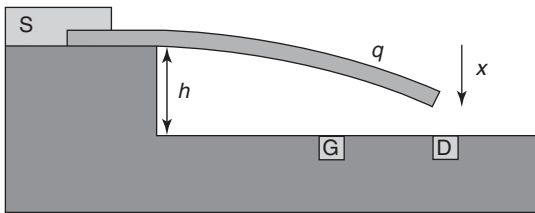

Figure 5
Schematic diagrams of a CNT nanorelay device. Reprinted with permission from Kinaret J, *et al.* 2003 A carbon nanotube based nanorelay. *Appl. Phys. Lett.* **82**, 1287–9. Copyright 2003, American Institute of Physics.
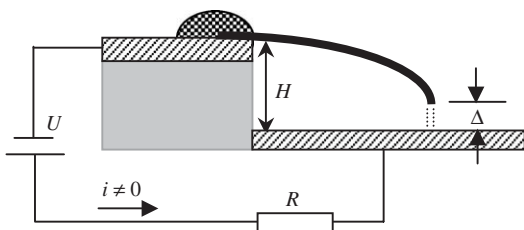

Figure 6
Schematic of nanotube-based device with tunneling contacts. Reprinted with permission from Ke C-H, Espinosa H D 2004 Feedback controlled nanocantilever device. *Appl. Phys. Lett.* **85**, 681–3. Copyright 2004, American Institute of Physics.

based on the interaction of the elastic energy, van der Waals energy and the electrostatic energy, as well as the feedback control mechanism through the resistor R in the device circuit. The representative characteristic curve of the device is shown in Fig. 7. At the "upper" equilibrium position, the electrostatic force is balanced by the elastic force from the deflection of the nanotube. There is no current in the circuit—"OFF" state. With the increase in applied voltage, the nanotube cantilever is pulled-in inducing tunneling contact with the bottom electrode. The "lower" equilibrium position is reached with a tunneling gap between the tip and electrode which is determined by the
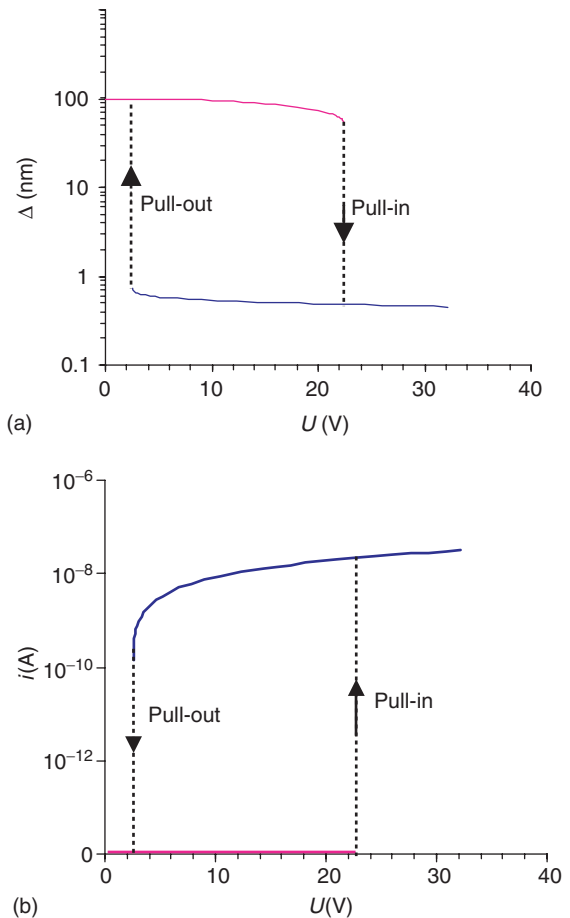

Figure 7
Representative characteristic of pull-in and pull-out processes for the feedback-controlled nanocantilever device. (a) Relationship between the gap Δ and the applied voltage U. (b) Relationship between the current i in the circuit and the applied voltage U. Reprinted with permission from Ke C-H, Espinosa H D 2004 Feedback controlled nanocantilever device. *Appl. Phys. Lett.* **85**, 681–3. Copyright 2004, American Institute of Physics.

voltage applied on the gap adjusted by the feedback resistor R. There is stable current in the device—"ON" state. These two states can be switched through the pull-in and pull-out processes by controlling the applied voltage U. The potential applications of the device include ultrasonic wave detection for monitoring the health of materials and structures, gap sensing, NEMS switches, memory elements, and logic devices.

The current jump behavior at pull-in has been confirmed by means of *in situ* SEM experiments. In this experiment, a nanotube cantilever, freestanding above an electrode, was actuated by electrostatic forces (Ke *et al*. 2005a, 2005b) as shown in Fig. 8. The measured *I–V* behavior after the pull-in was found in very good agreement with the theoretical

prediction. The parameters used in the theoretical prediction include the length of the nanotube, $L = 3.8\,\mu m$; the diameter of the nanotube, $R_{ext} = 20\,nm$; initial gap between the nanotube cantilever and the electrode, $H = 200\,nm$; resistor resistance, $R = 0.98\,G\Omega$; and contact resistance, $R_0 = 50\,\Omega$ (Ke and Espinosa 2004).

In comparison to nanorelays (Kinaret *et al*. 2003, Lee *et al*. 2004), the device reported in Ke and Espinosa (2004) is a two-terminal device, which provides more flexibility in terms of device realization and control. In comparison to the NRAM described in Rueckes *et al*. (2000), the feedback-controlled NEMS device (Ke and Espinosa 2004) employs an electrical circuit incorporated with a resistor to adjust the electrostatic field and achieve a second stable equilibrium position. This feature reduces the constraints in fabricating devices with nanometer gap control between the freestanding CNTs or NWs and the substrate, and therefore, provides more reliability and tolerance to variability in fabrication parameters. However, the drawback of the feedback-controlled device, in memory applications, is that the memory becomes volatile. Hence, the working principle and the potential applications for these two devices are somewhat complementary.
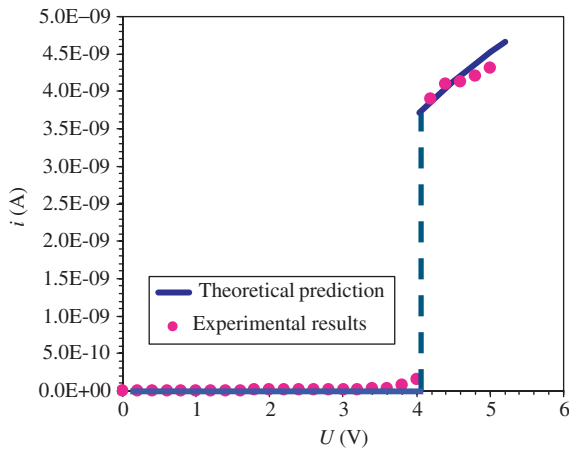

Figure 8
Comparison between theoretical prediction and *I–V* measurement of an electrostatically actuated freestanding nanotube cantilever with an electronic circuit incorporating a resistor.
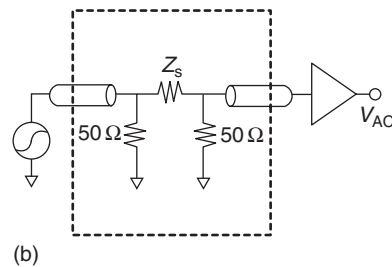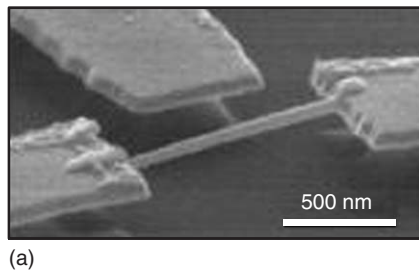
2.2 Nanowire-based NEMS Devices

(a) Resonators. Figure 9(a) shows a suspended platinum nanowire resonator, reported by Husain *et al*. (2003), and Fig. 9(b) the circuit used for magnetomotive drive and detection of its motion. The free standing platinum structure with a diameter of 43 nm and length of 1.3 μm was fabricated by random dispersion followed by e-beam lithography. A magnetomotive detection scheme (see Fig. 9(b)), in which an AC current drives a beam in a transverse magnetic field, was used to drive and read out the resonators. The measured quality factor Q was ~8500 and decreased slightly with the increase in magnetic field. It

Figure 9
(a) SEM image of the suspended nanowire device, 1.3 μm long and 43 nm in diameter. (b) Measurement circuit used for magnetomotive drive and detection. Reprinted with permission from Husain A, *et al*. 2003 Nanowire-based very-high-frequency electromechanical resonator. *Appl. Phy. Lett*. **83**, 1240–2. Copyright 2003, American Institute of Physics.

was noted that the response of the beam was in the linear regime. Badzey *et al*. (2004) reported a doubly clamped nanomechanical Si beam working in the nonlinear response region. The nonlinear response of the beam displays notable hysteresis and bistability in the amplitude–frequency space when the frequency sweeps upward and downward. This particular behavior shows that the device can be used as mechanical memory elements.

(b) Nanoelectromechanical programmable read-only memories. A germanium-nanowire-based nanoelectromechanical programmable read-only memory (NEMPROM) was reported by Ziegler *et al*. (2004). The device has two well-defined states because of the interplay of the electrostatic energy, van der Waals energy, and elastic energy. The electrostatic forces pull in the nanowire to make contact with the electrode (''ON'' state) and keep the state even without the electrostatic field because the van der Waals force is larger than the electrostatic force. The NEMPROM device can be switched OFF by mechanical motion or by heating the device above the stability limit to overcome the van der Waals attractive forces. The working principle of the NEMPROM is similar to that of the NRAM (Rueckes *et al*. 2000) since both of them employ van der Waals energy to achieve the bistability behavior, although the usage of germanium may provide better size control and electrical behavior than that of carbon nanotube.

3. Mutiphysics Modeling of NEMS

The design of NEMS depends on a thorough understanding of the mechanics of the devices themselves and the interactions between the devices and the external forces/fields. With the critical dimension shrinking from micron to nanometer scales, new physics emerges so that the theory typically applied to MEMS does not immediately translate to NEMS. For example, van der Waals forces from atomic interactions play an important role in NEMS, while they can be generally neglected in MEMS. Many NEMS devices can be modeled either as biased cantilever beams as fixed–fixed beams freestanding over a ground substrate. The beams can be carbon nanotubes, nanowires, or small nanofabricated parts. In the following section, we overview the governing equation of equilibrium for both small deformation and finite deformation based on continuum theory.

3.1 Governing Equations

The electromechanical characteristic of nanotube cantilevers or doubly clamped nanotube beams can be determined by coupling the van der Waals, electrostatic, and elastic forces. The governing equation under the small deformation assumption (considering only bending) is given by Desquesnes *et al*. (2002)

$$EI\frac{\mathrm{d}^4 r}{\mathrm{d}x^4} = q_{\mathrm{elec}} + q_{\mathrm{vdw}} \tag{1}$$

where r is the gap between the nanotube and the ground plane, x is the position along the tube, E is the Young's modulus (for carbon nanotube $E = 1$–$1.2\,\mathrm{TPa}$), I is the moment of inertia (for nanotubes, $I = \pi/4\left(R_{\mathrm{ext}}^4 - R_{\mathrm{int}}^4\right)$, R_{ext} and R_{int} are the outer and inner radii of the nanotubes, respectively), q_{elec} is the electrostatic force per unit length force, and q_{vdw} is the van der Waals force per unit length. q_{elec} is given by (Ke *et al*. 2005a, 2005b)

$$q_{\mathrm{elec}} = \frac{-\pi\varepsilon_0 V^2}{\sqrt{r(r + 2R_{\mathrm{ext}})}a\cosh^2(1 + (r/R_{\mathrm{ext}}))}(1 + f_{\mathrm{c}}) \tag{2}$$

where $f_{\mathrm{c}} = 0.85[(H + R_{\mathrm{ext}})^2 R_{\mathrm{ext}}]^{1/3}\delta(x - x_{\mathrm{tip}})$ accounts for the concentrated charge at the end of the tube (for doubly clamped tube, $f_{\mathrm{c}} = 0$) (Ke and Espinosa 2005), $\varepsilon_0 = 8.854 \times 10^{-12}\,\mathrm{C^2\,N^{-1}\,m^{-2}}$ is the permittivity of vacuum, V is the bias voltage, q_{vdw} can be calculated based on the continuum Lennard-Jones potential by assuming that the substrate is layers of graphite sheets (Desquesnes *et al*. 2002, 2004). It is noted that the van der Waals force is only relevant when the gap between nanotube and the substrate is in the order of a few nanometers.

For cantilevers exhibiting large displacements, as shown in Fig. 10(a), the curvature of the deflection should be considered and the governing equation changes into (Ke *et al*. 2005a, 2005b)

$$EI\frac{\mathrm{d}^2}{\mathrm{d}x^2}\left(\frac{\mathrm{d}^2 r/\mathrm{d}x^2}{\left(1 + (\mathrm{d}r/\mathrm{d}x)^2\right)^{3/2}}\right)$$
$$= (q_{\mathrm{vdw}} + q_{\mathrm{elec}})\sqrt{1 + \left(\frac{\mathrm{d}r}{\mathrm{d}x}\right)^2} \tag{3}$$

For doubly clamped structures exhibiting finite kinematics (Fig. 10(b)), stretching becomes significant as a consequence of the rope-like behavior of a doubly clamped nanotube. The corresponding governing equation is expressed as (Desquesnes *et al*. 2004, Ke *et al*. 2005a, 2005b, Pugno *et al*. 2005)

$$EI\frac{\mathrm{d}^4 r}{\mathrm{d}x^4} - \frac{EA}{2L}\int_0^L \left(\frac{\mathrm{d}r}{\mathrm{d}x}\right)^2 \mathrm{d}x\frac{\mathrm{d}^2 r}{\mathrm{d}x^2} = q_{\mathrm{elec}} + q_{\mathrm{vdw}} \tag{4}$$

where the term $EA/2L\int_0^L (\mathrm{d}r/\mathrm{d}x)^2\,\mathrm{d}x$ is the tension along the axis of the tube due to stretching.

The aforementioned governing equations can be numerically solved by either direct integration or finite difference method. The effect of various factors, such as concentrated charge, finite kinematics, and stretching, on the prediction of pull-in voltages of devices can then be identified.
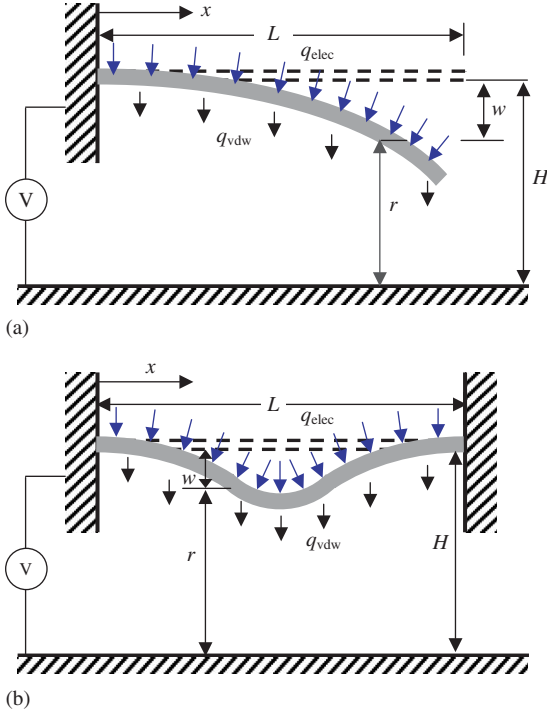
Figure 10
(a) Schematic of finite kinematics configuration of a cantilever nanotube device and (b) doubly clamped nanotube device subjected to electrostatic and van der Waals forces. Reproduced from Ke C-H, *et al.* 2005a Numerical analysis of nanotube based NEMS devices. Part II: Role of finite kinematics, stretching and charge concentrations. *J. Appl. Mech.* **72**, 726–31, with permission from The American Society of Mechanical Engineers.

3.2 Analytical Solutions

In this section, we discuss the electromechanical characteristic of the NEMS devices consisting of both cantilever and double-clamped nanotubes. In particular, the pull-in voltage calculations based on the energy method are reported (Ke *et al.* 2005a, 2005b, Pugno *et al.* 2005).

For nanotube cantilevers (singly clamped), the deflection of the cantilever nanotube can be approximated by the following quadratic function (Ke *et al.* 2005a, 2005b):

$$w(x) \approx \frac{x^2}{L^2} c \qquad (5)$$

where L is the length of the nanotube, c is a constant that represents the displacement of the end of the cantilever, and x is the coordinate along the nanotube.

By assuming that the nanotube's (external) radius R_{ext} is much smaller than the distance r between the

nanotube and ground plane, that is, $R_{ext}/r \ll 1$, the pull-in voltage, considering the nonlinear finite kinematics and the concentrated charges at the free end, is given by Ke *et al.* (2005a, 2005b)

$$V_{S\ PI} \approx k_S \sqrt{\frac{1 + K_S^{FK}}{1 + K_S^{tip}}} \frac{H}{L^2} \ln\left(\frac{2H}{R_{ext}}\right) \sqrt{\frac{EI}{\varepsilon_0}} \qquad (6a)$$

$$k_S \approx 0.85, \quad K_S^{FK} \approx \frac{8H^2}{9L^2}$$

$$K_S^{tip} \approx \frac{2.55\left[R_{ext}(H + R_{ext})^2\right]^{1/3}}{L} \qquad (6b)$$

where subscripts S refer to singly clamped boundary conditions for cantilevers, superscript FK refers to finite kinematics, tip refers to the charge concentration being at the free end.

For doubly clamped nanotubes, the deflection $w(x)$ is assumed such that it satisfies the boundary conditions $w(x = 0, L) = w(x = 0, L) = 0$, namely (Pugno *et al.* 2005)

$$w(x) \approx 16\left[\left(\frac{x}{L}\right)^2 - 2\left(\frac{x}{L}\right)^3 + \left(\frac{x}{L}\right)^4\right] c \qquad (7)$$

where $w(x = L/2) = c$ is here an unknown constant that represents the displacement of the central point. The pull-in voltage can be expressed as (Pugno *et al.* 2005)

$$V_{D\ PI} = k_D \sqrt{1 + k_D^{FK}} \frac{H + R}{L^2} \ln\left(\frac{2(H + R)}{R}\right) \sqrt{\frac{EI}{\varepsilon_0}} \qquad (8a)$$

$$k_D = \sqrt{\frac{1024}{5\pi S'(c_{PI})}\left(\frac{c_{PI}}{H + R}\right)}, \quad k_D^{FK} = \frac{128}{3003}\left(\frac{c_{PI}}{\rho}\right)^2 \qquad (8b)$$

$$\rho^2 = \frac{I}{A} = \frac{R_{ext}^2 + R_{int}^2}{4}$$

$$S(c) = \sum_{i=1}^{\infty}\left(\frac{1}{(\ln(2(H + R)/R))^i}\sum_{j=i}^{\infty} a_{ij}\left(\frac{c}{(H + R)}\right)^j\right) \qquad (8c)$$

Subscripts D refer to double clamped boundary conditions, c_{PI} is the central deflection of the nanotube at the pull-in, and the $\{a_{ij}\}$ in Eqn. (8c) are known constants (Pugno *et al.* 2005).

The accuracy of the analytical solutions is verified by comparison with both numerical integration of the governing equations (Desquesnes *et al.* 2002, Ke *et al.* 2005a, 2005b) and experimental measurements (see Sect. 3.3) (Ke *et al.* 2005a, 2005b). The comparison between pull-in voltages evaluated numerically and theoretically for doubly (D) and singly (S) clamped nanotube devices is listed in Table 1 (Ke *et al.* 2005a, 2005b). Columns six and seven in Table 1 compare

Table 1
Comparison between pull-in voltages evaluated numerically and theoretically for doubly (D) and singly (S) clamped nanotube devices, respectively. $E = 1$ TPa, $R_{int} = 0$.

Case	BC	H (nm)	L (nm)	$R = R_{ext}$ (nm)	V_{PI} (V) (theo.linear)	V_{PI} (V) (num. linear)	V_{PI} (V) (theo. non-linear)	V_{PI} (V) (num. non-linear)
1	D	100	4000	10	3.20	3.18	9.06	9.54
2	D	100	3000	10	5.69	5.66	16.14	16.95
3	D	100	2000	10	12.81	12.73	36.31	38.14
4	D	150	3000	10	9.45	9.43	38.93	40.92
5	D	200	3000	10	13.53	13.52	73.50	77.09
6	D	100	3000	20	19.21	18.74	31.57	32.16
7	D	100	3000	30	38.57	37.72	51.96	50.63
8	S	100	500	10	27.28 (w)	27.05 (w)	27.52 (w)	27.41 (w)
9	S	100	500	10	27.28 (w)	27.05 (w)	30.87	31.66

For a cantilever nanotube device the symbol (w) denotes that the effect of charge concentration has been included.
Reproduced from Ke C-H, *et al.* 2005a Numerical analysis of nanotube based NEMS devices. Part II: Role of finite kinematics, stretching and charge concentrations. *J. Appl. Mech.* **72**, 726–31, with permission from The American Society of Mechanical Engineers.

analytical and numerical pull-in voltage predictions under the assumption of small deformations. Columns eight and nine in Table 1 compare analytical and numerical pull-in voltage predictions under the assumption of finite kinematics. The agreement is very good (with a maximum discrepancy of 5%).

3.3 Comparison between Analytical Predictions and Experiments. In this section, a comparison between analytical predictions and experimental data, for both small deformation and finite kinematics regimes, is presented.

(a) Small deformation regime. The nanotweezers experimental data reported by Akita *et al.* (2001), plotted in Fig. 11, is used to assess the model accuracy under small deformation. In this case, the nanotweezers are equivalent to a nanotube cantilever with length of 2.5 μm freestanding above an electrode with a gap of 390 nm.Symmetry is here exploited. In the same figure, a comparison between the analytically predicted nanotube cantilever deflection and the experimentally measured data is shown (Ke *et al.* 2005a, 2005b). The analytical model includes the van der Waals force and charge concentration at the free end of the nanotube cantilever. Model parameters include Young's modulus, $E = 1$ TPa, external radius $R = R_{ext} = 5.8$ nm, and $R_{int} = 0$. The pull-in voltage from the analytical model is 2.34 V while the experimentally measured pull-in voltage was 2.33 V. It is clear that the analytical prediction and experimental data for the deflection of the nanotube cantilever, as a function of applied voltage, are in very good agreement.

(b) Finite kinematics regime. Experimental data corresponding to the deflection of carbon nanotube cantilevers in the finite kinematics regime were recently obtained by *in situ* SEM measurements
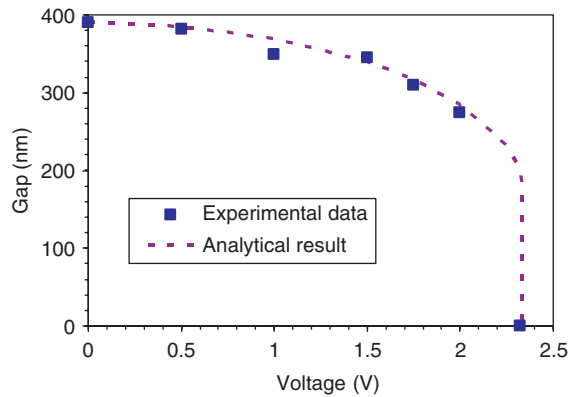

Figure 11
Comparison between experimental data and theoretical prediction in the small deformation regime. Reproduced from Ke C-H, *et al.* 2005b Experiments and modeling of nanotube NEMS devices. *J. Mech. Phys. Solids* **53**, 1314–33, with permission from Elsevier.

(Ke *et al.* 2005a, 2005b). An MWNT mounted to a manipulator probe as a cantilever was placed parallel to an electrode and actuated by the electrostatic force. The length of the nanotube is 6.8 μm and the gap between the nanotube and the electrode is 3 μm. Because the ratio between the length of the nanotube and the gap between the nanotube and electrode is 2.3, the deflection of the nanotube can be considered to be in the finite kinematics regime.

The experimentally measured nanotube cantilever deflections, in the finite kinematics regime, are plotted in Fig. 12 (Ke *et al.* 2005a, 2005b). The figure also shows a comparison between analytical prediction and experimental data. The analytical model includes finite kinematics, the van der Waals force, and charge concentration at the free end of the nanotube
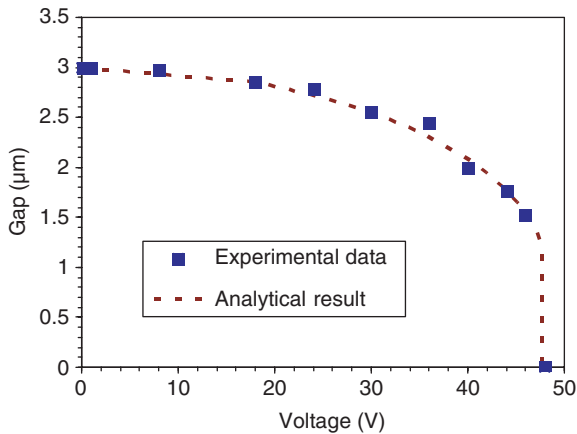
Figure 12

Comparison between experimental data and theoretical prediction in the finite kinematics regime. Reproduced from Ke C-H, *et al.* 2005b Experiments and modeling of nanotube NEMS devices. *J. Mech. Phys. Solids* **53**, 1314–33, with permission from Elsevier.

cantilever. For these predictions, the following parameters were employed: length of the nanotube, $L = 6.8\,\mu m$, initial gap between nanotube and electrode, $H = 3\,\mu m$, $R = R_{ext} = 23.5\,nm$, $R_{int} = 0$, $E = 1\,TPa$. The pull-in voltage given by the analytical analysis is 47.8 V, whereas the pull-in voltage experimentally measured was 48 V.

Bibliography

Akita S, Nakayama Y, Mizooka S, Takano Y, Okawa T, Miyatake Y, Yamanaka S, Tsuji M, Nosaka T 2001 Nanotweezers consisting of carbon nanotubes operating in an atomic force microscope. *Appl. Phys. Lett.* **79**, 1691–3

Badzey R L, Zolfagharkhani G, Gaidarzhy A, Mohanty P 2004 A controllable nanomechanical memory element. *Appl. Phys. Lett.* **85**, 3587–9

Davis Z J, Abadal G, Kuhn O, Hansen O, Grey F, Boisen A 2000 Fabrication and characterization of nano-resonating devices for mass detection. *J. Vac. Sci. Technol. B* **18**, 612–6

Desquesnes M, Rotkin S V, Alaru N R 2002 Calculation of pull-in voltages for carbon-nanotube-based nanoelectromechanical switches. *Nanotechnology* **13**, 120–31

Desquesnes M, Tang Z, Aluru N R 2004 Static and dynamic analysis of carbon nanotube-based switches. *J. Eng. Mater. Tech.* **126**, 230–7

Fennimore A M, Yuzvlnsky T D, Han W Q, Fuhrer M S, Cummings J, Zettl A 2003 Rotational actuators based on carbon nanotubes. *Nature* **424**, 408–10

Husain A, Hone J, Postma H W Ch, Huang X M H, Drake T, Barbic M, Scherer A, Roukes M L 2003 Nanowire-based very-high-frequency electromechanical resonator. *Appl. Phys. Lett.* **83**, 1240–2

Ilic B, Craighead H G, Krylov S, Senaratne W, Ober C, Neuzil P 2000 Attogram detection using nanoelectromechanical oscillators. *J. Appl. Phys.* **95**, 3694–703

Ke C-H, Espinosa H D 2004 Feedback controlled nanocantilever device. *Appl. Phys. Lett.* **85**, 681–3

Ke C-H, Espinosa H D 2005 Numerical analysis of nanotube based NEMS devices. Part I: Electrostatic charge distribution on multiwalled nanotubes. *J. Appl. Mech.* **72**, 721–5

Ke C-H, Espinosa H D, Pugno N 2005a Numerical analysis of nanotube based NEMS devices. Part II: Role of finite kinematics, stretching and charge concentrations. *J. Appl. Mech.* **72**, 726–31

Ke C-H, Pugno N, Peng B, Espinosa H D 2005b Experiments and modeling of nanotube NEMS devices. *J. Mech. Phys. Solids.* **53**, 1314–33

Kim P, Lieber C M 1999 Nanotube nanotweezers. *Science* **126**, 2148–50

Kinaret J, Nord T, Viefers S 2003 A carbon nanotube based nanorelay. *Appl. Phys. Lett.* **82**, 1287–9

Lee S, Lee D, Morjan R, Jhang S, Sveningsson M, Nerushev O, Park Y, Campbell E 2004 A three-terminal carbon nanorelay. *Nano Lett.* **4**, 2027–30

Pugno N, Ke C-H, Espinosa H D 2005 Analysis of doubly clamped nanotube devices in the finite deformation regime. *J. Appl. Mech.* **72**, 445–9

Roukes M L 1999 Yoctocalorimetry: phonon counting in nanostructures. *Physica B* **263-4**, 1–15

Roukes M L 2004 Nanoelectromechanical Systems, Technical Digest of the 2000 Solid-State Sensor and Actuator Workshop.

Rueckes T, Kim K, Joslevich E, Tseng G Y, Cheung C, Lieber C M 2000 Carbon nanotube-based nonvolatile random access memory for molecular computing. *Science* **289**, 94–7

Sazonova V, Yaish Y, Üstünel H, Roundy D, Arias T, McEuen P 2004 A tunable carbon nanotube electromechanical oscillator. *Nature* **431**, 284–7

Ziegler K J, Lyons D M, Holmes J D, Erts D, Polyakov B, Olin H, Svensson K, Olsson E 2004 Bistable nanoelectromechanical devices. *Appl. Phys. Lett.* **84**, 4074–6

H. D. Espinosa, C. Ke, and N. Pugno